Energy & Environmental Science

Cite this: *Energy Environ. Sci.*, 2012, **5**, 6345

www.rsc.org/ees

PAPER

Photocatalytic H_2 production on Pt/TiO_2–SO_4^{2-} with tuned surface-phase structures: enhancing activity and reducing CO formation

Yi Ma,[ab] Qian Xu,[a] Xu Zong,[a] Donge Wang,[ab] Guopeng Wu,[a] Xiang Wang[ab] and Can Li*[a]

Received 1st July 2011, Accepted 5th August 2011
DOI: 10.1039/c1ee02053f

Photocatalytic reforming of biomass is a promising way to produce hydrogen using renewable energy. Photocatalytic reforming of methanol on Pt/TiO_2–SO_4^{2-} as a model reaction of biomass reforming was investigated. Sulfated TiO_2 (TiO_2–SO_4^{2-}) with a tunable surface phase was prepared by calcining commercially available titanium dioxide TiO_2 (Degussa P25) with deposited sodium sulfate Na_2SO_4 as a modifier. Compared with P25, the as-prepared TiO_2–SO_4^{2-} with Pt co-catalyst shows an increase up to 6-fold in the activity for H_2 production *via* photocatalytic reforming of methanol, and the CO (undesired product) concentration in the produced H_2 is decreased by about two orders of magnitude. XRD patterns and UV Raman spectra clearly indicate that TiO_2 depositing with Na_2SO_4 can significantly retard the phase transformation from anatase to rutile during calcination at elevated temperatures. It is proposed that both the phase composition and the high crystallinity of TiO_2 contribute to the high H_2 evolution activity. IR spectra of pyridine adsorption and the NH_3-TPD profile show that the surface acid sites of the photocatalyst are greatly reduced after calcination at high temperatures. It is proposed that the decrease in the acidity of the samples might be responsible for the low CO selectivity.

1. Introduction

Energy security due to the depletion of fossil fuel reserves and the environmental issues caused by the excessive CO_2 emission from fossil fuel based power generation have received ever increasing attention throughout the world. Efficient hydrogen production is one of the key technologies for the current clean energy developments.[1–3] Currently, about 95% of the hydrogen production worldwide is from fossil fuels such as natural gas and coal, mainly by steam reforming,[4] which consumes large amounts of additional energy. One of the promising alternative routes of hydrogen generation from clean and renewable energy sources is the photocatalytic hydrogen production *via* reforming of biomass. Methanol as a model compound of biomass has been intensively investigated for the H_2 production *via* thermal catalytic reforming[5–8] and also recently *via* photocatalytic reforming.[9–13]

Thus far, titania-based catalyst as one of the most suitable semiconductor photocatalysts has been extensively investigated.

[a]*State Key Laboratory of Catalysis, Dalian Institute of Chemical Physics, Dalian National Laboratory for Clean Energy, Chinese Academy of Sciences, 457 Zhongshan Road, Dalian, 116023, China. Web: http://www.canli.dicp.ac.cn; E-mail: canli@dicp.ac.cn; Fax: +86-411-84694447; Tel: +86-411-84379070*
[b]*Graduate University of Chinese Academy of Sciences, Beijing, 100049, China*

Broader context

Photocatalytic H_2 production *via* biomass reforming is a promising technology in the renewable energy utilization. An efficient utilization of H_2 requires both the high production activity and the high purity of H_2. As in the fuel cell, the CO concentration in H_2 should be controlled to an extremely low level. Therefore, in this article, two issues, H_2 production activity and CO selectivity, have been investigated. TiO_2-based catalyst is one of the most suitable semiconductor photocatalysts. It is believed that the phase structure especially the surface-phase junction can significantly affect the activity of TiO_2. Here, a series of TiO_2 catalysts with tuned surface phase structures were prepared by calcining a commercially available TiO_2 (P25) with deposited Na_2SO_4. The mixed phase structure of TiO_2 can be obtained at high temperature using this method. The high H_2 production activity and the low CO selectivity of the catalysts were achieved by tuning the phase structure of TiO_2. The phase structure and the surface acidity of the TiO_2-based catalysts have been proved to be the crucial reasons for the excellent performance of the catalysts in photocatalytic reforming of methanol.

The photocatalytic activity of titanium dioxide (TiO_2) varies widely with its crystal structure, crystallinity and particle size. It is believed that the crystal structure and the composition of titania can significantly affect the photocatalytic activity.[14–16] In our previous research, it was found that the optimized photocatalytic activity of titania can be obtained not from anatase or rutile but from a mixture of the two phases, which was ascribed to the formation of a surface-phase junction between anatase and rutile.[17] Furthermore, surface-phase junction has provided a guidance in the photocatalyst preparation. Very recently, we have found that the phase structure of TiO_2 can be successfully controlled *via* a careful calcination of commercially available TiO_2 (P25), and the photocatalytic activity for hydrogen production *via* biomass reforming can be significantly enhanced.[18]

Various methods have been employed to control the crystal phases of TiO_2.[19–23] Yan *et al.*[24] found that the contents of anatase and rutile phases in TiO_2 powder can be controlled by simply changing the proportion of Cl^- and SO_4^{2-} in the aqueous phase of the microemulsion *via* the hydrothermal preparation method. However, this method leads to a relatively low crystallinity of TiO_2. Colon *et al.*[25] used a sol–gel method to synthesize the sulfated TiO_2. They found that SO_4^{2-} can maintain the anatase phase of TiO_2. Until now, almost all the sulfated TiO_2 reported in the literature were used in the photocatalytic oxidation of pollutants. The research on the photocatalytic H_2 production using sulfated TiO_2 has not been reported.

In addition, another issue in photocatalytic reforming of methanol is the formation of carbon monoxide as a by-product. The presence of trace CO in hydrogen can be a serious problem in the application of H_2, such as in the proton exchange membrane fuel cells (PEMFCs). PEMFC has a very low CO tolerance; the Pt-based anode in a PEMFC can be seriously poisoned even with trace CO (5–100 ppm) present in the hydrogen stream.[26,27] Therefore, a high activity of H_2 production with an ultra low CO formation is highly desired in the photocatalytic reforming of methanol.

In this work, we report that the photocatalyst Pt/TiO_2–SO_4^{2-} not only increases the H_2 production activity, up to 6-fold compared with Pt/P25, but also shows a dramatic decrease in the CO concentration of the produced H_2, by about two orders of magnitude. It is proposed that both the surface phase structure and the surface acidity/basicity properties contribute to the excellent performance in the hydrogen production *via* photocatalytic reforming of methanol on Pt/TiO_2–SO_4^{2-}.

2. Experimental

2.1. Catalyst preparation

All reagents used in the investigations are of analytical grade without further purification. P25-SO_4^{2-} samples containing different amounts of SO_4^{2-} were prepared using an impregnation method. The commercially available TiO_2 (Degussa P25) was dispersed uniformly in three types of solutions, *i.e.* a sodium sulfate aqueous solution, sulfuric acid aqueous solution and potassium sulfate aqueous solution. The formed slurry samples were left overnight and continuously stirred for sufficient impregnation before they were dried in a water bath. Then, the samples were kept in an oven at 80 °C for 3 h. After that, the samples were ground and calcined in a muffle furnace at different temperatures for 3 h. The as-prepared samples are denoted as P25-*x*%SO_4^{2-}-T, P25-*x*%SO_4^{2-}-T(H_2SO_4) and P25-*x*%SO_4^{2-}-T(K_2SO_4), when using sodium sulfate, sulfuric acid and potassium sulfate aqueous solution, respectively. The *x* denotes the mass percentage of SO_4^{2-} that was initially added in TiO_2 and the *T* indicates the calcination temperature in degrees Celsius (°C). For the purpose of comparison, P25 was treated in deionized water instead of sulfate solution denoted as P25-H_2O-T. Again, *T* is the calcination temperature.

2.2. Photocatalytic experiments

Experiments on photocatalytic reaction were carried out in a Pyrex reaction cell which was connected to a closed gas circulation and a vacuum system. A 300 W top-irradiated Xenon lamp was used as a light source. Prior to illumination, the system was always deaerated by evacuation in order to remove the air from the system.

The gaseous products from methanol reforming, such as H_2, CH_4, CO and CO_2, were analyzed by an online gas chromatography. The amount of hydrogen produced was measured by a thermal conductivity detector, and CO was detected by a flame ionization detector after it was converted into CH_4 in a methanator. In the experiments, the sampling and online analyzing were performed once an hour. Typically, 0.1 g of the catalyst was suspended in a 200 ml methanol solution (20 vol%); 0.05 wt% Pt was loaded as a co-catalyst on TiO_2 at the very beginning of the reaction by an *in situ* photodeposition method from the precursor $H_2PtCl_6 \cdot 6H_2O$ solution under irradiation.

2.3. Catalyst characterization

The phase compositions in the bulk and surface regions of the samples were characterized using XRD and UV Raman spectroscopy. XRD patterns were obtained on a Rigaku D/Max-2500/PC powder diffraction system with a CuKα radiation source (40 kV and 100 mA) at room temperature. Diffraction patterns were collected from 20° to 80° at a rate of 5° min^{-1}. UV Raman spectra were collected on a home-made Raman spectrograph system; the spectrograph is a triple-stage dispersed-subtractive spectrograph, in which the first two stages are used to cut off the Rayleigh line and the third one is used to collect Raman spectra using a CCD detector. The scattered lights were collected by the ellipse collecting mirror in a back-scattering geometry and focused into the entrance of the Raman spectrograph. The Raman spectra were recorded with a spectral resolution of 2 cm^{-1} with the laser excitation at 325 nm from He–Cd Laser.

The BET surface area of the samples was measured based on nitrogen adsorption at 77 K using a Micromeritics ASAP 2000 adsorption analyzer.

TEM images were obtained using a Tecnai G^2 Spirit (FEI company) at an acceleration voltage of 120 kV. HRTEM images were obtained on Tecnai G^2 F30 S-Twin (FEI company) with an acceleration voltage of 300 kV.

Infrared spectra of pyridine adsorption were measured with a resolution of 4 cm^{-1} and 32 scans on a Fourier transform

infrared spectrometer (Nicolet NEXUS 470). The experiments were carried out in a special IR cell in conjunction with a water-cooling system and a vacuum system. There are several steps in the experimental procedure. The sample, typically 20 mg of titania, was first pressed into a self-supporting thin wafer (15 mm diameter) and then, it was moved into the sample holder of the IR cell. The wafer in the IR cell was evacuated for 1 h to remove the impurities in the cell, and then the background spectrum of the sample was recorded. After introducing the pyridine vapor for 15 min, the wafer was degassed under vacuum condition at 423 K for 30 min before the spectrum was recorded.

The NH_3-TPD (temperature programmed desorption) profiles were obtained by monitoring the NH_3 desorbed from the samples by GC. The sample, typically 140 mg of titania, was heated in a vacuum condition to 200 °C and kept for 3 h, and then cooled down to 150 °C. Pure NH_3 was then introduced into the sample. After adsorption, the system was evacuated. The sample was then heated up in a flowing He carrier gas from 150 °C to 750 °C at a rate of 20 °C min^{-1} and the amount of desorbed NH_3 was measured by a gas chromatograph (SHIMADZU).

3. Results and discussion

3.1. Phase composition of the TiO_2 adjusted by Na_2SO_4

Table 1 lists the physical details of the TiO_2, including the phase compositions in the bulk and surface regions and the BET surface area. The phase compositions in the bulk region of the samples are estimated from the integrated intensities of rutile (110) and anatase (101) diffractions in XRD patterns.[28–30] The phase compositions in the surface region are estimated from the UV Raman spectra according to the literature.[29]

Fig. 1(a) shows the XRD patterns of P25-x%SO_4^{2-}-700 with different amounts of SO_4^{2-} addition. The "A" and "R" in the figure denote the anatase and rutile phases, respectively. The XRD patterns show that the anatase phase in the P25-H_2O-700 nearly disappears, which indicates a complete phase transformation from anatase to rutile after calcination at 700 °C. Interestingly, XRD patterns indicate that the anatase phase can be detected even after the calcination at 700 °C when a very small amount, 0.1 wt%, of SO_4^{2-} is present. With increasing the amount of SO_4^{2-} from 0.1 wt% to 3.0 wt%, more anatase phase is remained after the calcination. Therefore, it is concluded that the phase transformation from anatase to rutile can be inhibited by the presence of Na_2SO_4 on the TiO_2 surface.

Table 1 Phase compositions in the bulk and surface regions and the BET surface area (S_{BET}) of the samples

	W_A[a]		
	Bulk region	Surface region	S_{BET}/m² g⁻¹
P25	87%	—	53.0
P25-H_2O-700	1%	2%	13.8
P25-0.1%SO_4^{2-}-700	3%	6%	15.4
P25-1.0%SO_4^{2-}-700	3%	7%	16.2
P25-1.0%SO_4^{2-}-700	16%	27%	20.0
P25-3.0%SO_4^{2-}-700	43%	75%	28.8

[a] W_A: weight fraction of anatase in TiO_2.

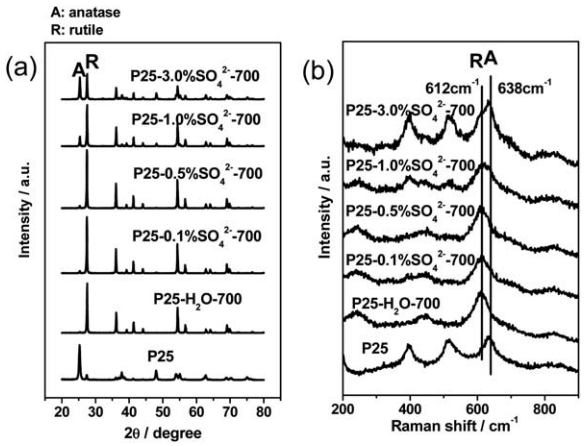

Fig. 1 (a) XRD patterns and (b) UV Raman spectra of P25-H_2O-700 and P25-x%SO_4^{2-}-700.

UV Raman spectroscopy is very sensitive to the surface phase of TiO_2 due to its intense absorption of UV light.[17,30,31] Fig. 1(b) shows the UV Raman spectra of P25-x%SO_4^{2-}-700. Two characteristic bands ascribed to anatase and rutile, have been observed at 638 cm^{-1} and 612 cm^{-1}, respectively. With increasing the amount of SO_4^{2-}, the intensity of the band at 638 cm^{-1} is becoming predominant, while the band at 612 cm^{-1} is gradually diminishing. Similar to the tendency of the increase in the anatase content estimated from the XRD patterns, the anatase phase in the surface region of the samples is well retained from 2% to about 75% as the amount of SO_4^{2-} increases from 0 to 3.0 wt%. The difference is that the anatase phase in the surface region is relatively more than it is in the bulk region of the samples.

The BET surface areas of the samples are also displayed in Table 1. It is noted that, after an impregnation treatment of P25 in water followed by calcination at 700 °C, the surface area of P25 is greatly decreased from 53.0 m^2 g^{-1} to 13.8 m^2 g^{-1}. The surface area of P25-H_2O-700 is the smallest among the samples. With increasing the amount of SO_4^{2-} up to 3.0 wt%, the surface areas of these samples increase from 13.8 m^2 g^{-1} to 28.8 m^2 g^{-1}. It is clearly shown that the BET surface areas are closely related to the content of anatase in the samples. The more the anatase content, the larger the surface area. These results imply that the phase transformation and the growth of the particle size are interrelated. The same phenomenon was reported by many other researchers.[32–34] The adsorbed SO_4^{2-} or other ions are actually on the surface defect sites of anatase particles, namely, the defect sites are coordinately saturated by the adsorbed anions. The phase transformation of TiO_2 starts from the solid state reaction between the anatase particles in the agglomerated TiO_2 particles.[29] When the defect sites are deactivated by the sulfate anions, the solid state reaction is inhibited and consequently the phase transformation from anatase to rutile is retarded.

3.2. Photocatalytic H_2 production on the sulfated TiO_2 catalysts

Photocatalytic reforming of CH_3OH to produce H_2 was performed under mild conditions. The Pt/P25 without any pre-treatment exhibits the lowest H_2 evolution rate compared with other pre-treated catalysts (Fig. 2(a)). The H_2 evolution rate is

significantly enhanced with increasing the amount of SO_4^{2-} in Pt/P25-x%SO_4^{2-}-700 and approaches to the maximum activity for Pt/P25-1.0%SO_4^{2-}-700. With further increasing the amount of SO_4^{2-} to 3.0 wt%, a slight decrease in the rate of hydrogen production is observed. The photocatalytic activity can be further optimized by changing the calcination temperature. As shown in Fig. 3(a), the highest photocatalytic activity can reach to 9530 μmol g^{-1} h^{-1} for Pt/P25-1.0%SO_4^{2-}-650 with only 0.05 wt % Pt as the co-catalyst, which is more than 6 times the activity of Pt/P25. When taking account of the surface area, the H_2 evolution rate per unit surface area is enhanced to over 15 times the activity of Pt/P25, see Fig. 2(b).

As we all know, the recombination of photo-induced electrons and holes in a photocatalyst is a major factor affecting the photocatalytic activity.[35] Usually, the defects in the bulk and surface regions of the semiconductor could be the recombination centers. The high crystallinity, which can be obtained by the high temperature calcination, can effectively reduce the defects. As presented in Fig. 2(a) and Fig. 3(a), all the samples calcined at high temperatures (above 600 °C in the experiments) can enhance the H_2 evolution activity by at least twice that of Pt/P25.

On the other hand, the surface microstructure of TiO_2, particularly the surface crystalline phase of TiO_2, substantially affects the photocatalytic activity of H_2 production. The anatase/rutile phase junction has been proved to be an important factor for the high photocatalytic activity.[17] As revealed in the literature,[36,37] the conduction band of TiO_2(A) is about 0.2 eV higher than that of TiO_2(R) which is thought to facilitate interfacial electron transfer from anatase to rutile. Other research observed the opposite phenomena, since the anatase trapping site is 0.8 eV lower in energy than the conduction band of anatase and is also below the conduction band of rutile, which allows the electron transfer from rutile to anatase.[38,39] Anyhow, the contact between anatase and rutile is beneficial for the charge separation. For P25, the insufficient contact between particles, originating from the high-temperature flame hydrolysis synthesis method and the improper ratio of the two phases, results in a lower activity compared with other catalysts tested. For the samples prepared in this work, a large amount of particles gradually agglomerated and transformed from anatase to rutile under high temperature treatment. This process is accompanied by the formation of the anatase/rutile phase junctions due to the uncompleted phase transformation. Obviously, a more intimate contact between anatase and rutile has been obtained using this method. Moreover, the amount of phase junctions can be controlled by the amount of SO_4^{2-} addition. UV Raman spectra show that the surface phase compositions of P25-1.0%SO_4^{2-}-700 are 27% anatase and 73% rutile. In this catalyst, the more exposed phase junctions result in a higher H_2 evolution activity. However, for P25-3.0%SO_4^{2-}-700, the activity is decreased somewhat, because more SO_4^{2-} addition leads to an excessive anatase phase, which

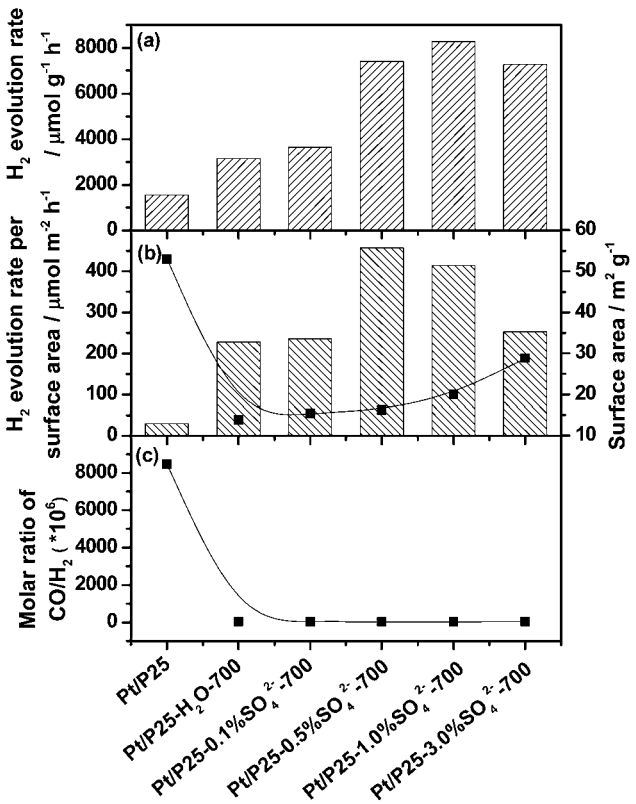

Fig. 2 (a) Overall photocatalytic activity of H_2 production and (b) surface-specific photocatalytic activity of H_2 production of Pt/P25, Pt/P25-H_2O-700 and Pt/P25-x%SO_4^{2-}-700. The solid line in (b) indicates the surface area of the samples. (c) CO selectivity of Pt/P25, Pt/P25-H_2O-700 and Pt/P25-x%SO_4^{2-}-700 catalysts. *Reaction conditions*: Catalyst, 0.1 g; Co-catalyst, 0.05 wt% Pt; Methanol aqueous solution, 200 ml (20 vol%); Light source, Xe-lamp (300 W).

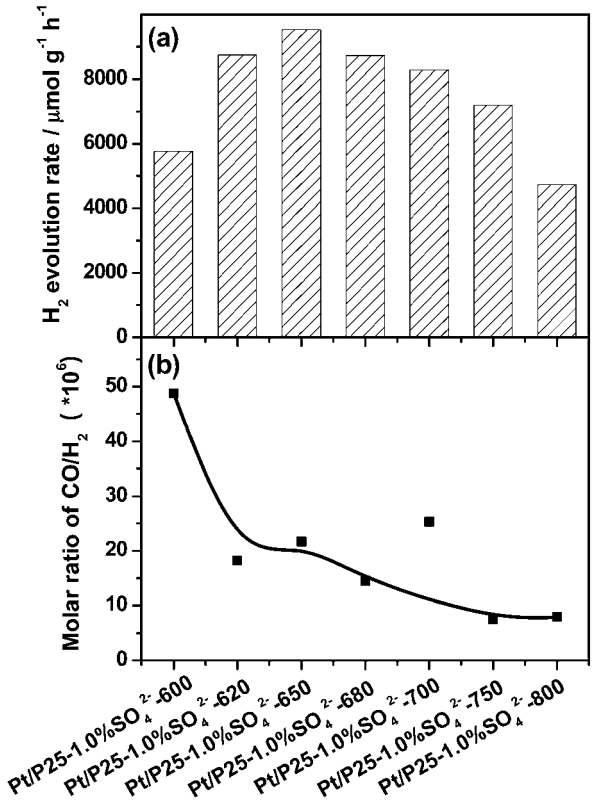

Fig. 3 (a) Rate of H_2 evolution and (b) CO selectivity of Pt/P25-1.0% SO_4^{2-}-T catalysts treated at different calcination temperatures. *Reaction conditions*: catalyst, 0.1 g; co-catalyst, 0.05 wt% Pt; methanol solution, 200 ml (20 vol%); light source, Xe-lamp (300 W).

may decrease the phase junctions exposed on the surface of the catalyst.

Fig. 4 displays the TEM and HRTEM images of the catalysts. The smaller particles in the images usually belong to the anatase phase and most of the larger ones belong to the rutile phase. The particle size of P25 (Fig. 4(a)) is in a range between 20 and 80 nm; the particles around 25 nm belong to the anatase phase and the larger ones around 60 nm belong to the rutile phase. For the samples of P25-H_2O-700 (Fig. 4(b)) and P25-0.1%SO_4^{2-}-700 (Fig. 4(c)), almost all the particles are around 100 nm and the particles below 50 nm are rarely found, suggesting a large amount of the rutile phase in the samples; while, for the samples of P25-0.5%SO_4^{2-}-700 (Fig. 4(d)) and P25-1.0%SO_4^{2-}-700 (Fig. 4(e)), smaller particles below 50 nm increasingly appear and a large amount of the smaller particles disperse on the edge of the larger particles, even grow together. The HRTEM image of P25-1.0%SO_4^{2-}-700 shows an example of the intimate contact between the anatase and rutile particles. As shown in Fig. 4(g), the round smaller particle exhibits fringes with a lattice spacing of *ca.* 3.51 Å and the long larger particle exhibits *ca.* 3.24 Å, which can be indexed into the (101) plane of anatase and (110) plane of rutile, respectively. It is clearly shown that the two particles grow together intimately. For the sample of P25-3.0% SO_4^{2-}-700 (Fig. 4(f)), smaller particles (below 50 nm) become dominant, which leads to less opportunity for forming anatase/rutile junctions due to the large amount of anatase particles.

3.3. The effect of Na^+ and SO_4^{2-} on the photocatalytic activity of TiO_2

In order to investigate the effect of Na^+ on the photocatalytic reaction, different cations in sulfate were examined. As shown in Fig. 5(a), the H_2 production activities of both Pt/P25-1.0%SO_4^{2-}-700(H_2SO_4) and Pt/P25-1.0%SO_4^{2-}-700(K_2SO_4) can be obviously enhanced compared with that of Pt/P25-H_2O-700. Clearly, the TiO_2 phase structure can be tuned by all these additives. It should be noted that the ability on anatase phase stabilization of different sulfates is different and it decreases in the order: K_2SO_4 > Na_2SO_4 > H_2SO_4, as shown in the XRD patterns (Fig. 5(b)). The larger molecule could prevent the anatase particles from agglomeration more efficiently than the smaller ones; thus, the different phase structures have been obtained. The H_2 production activities show that Na_2SO_4 is the most appropriate additive under the same experimental condition, as the anatase phase in

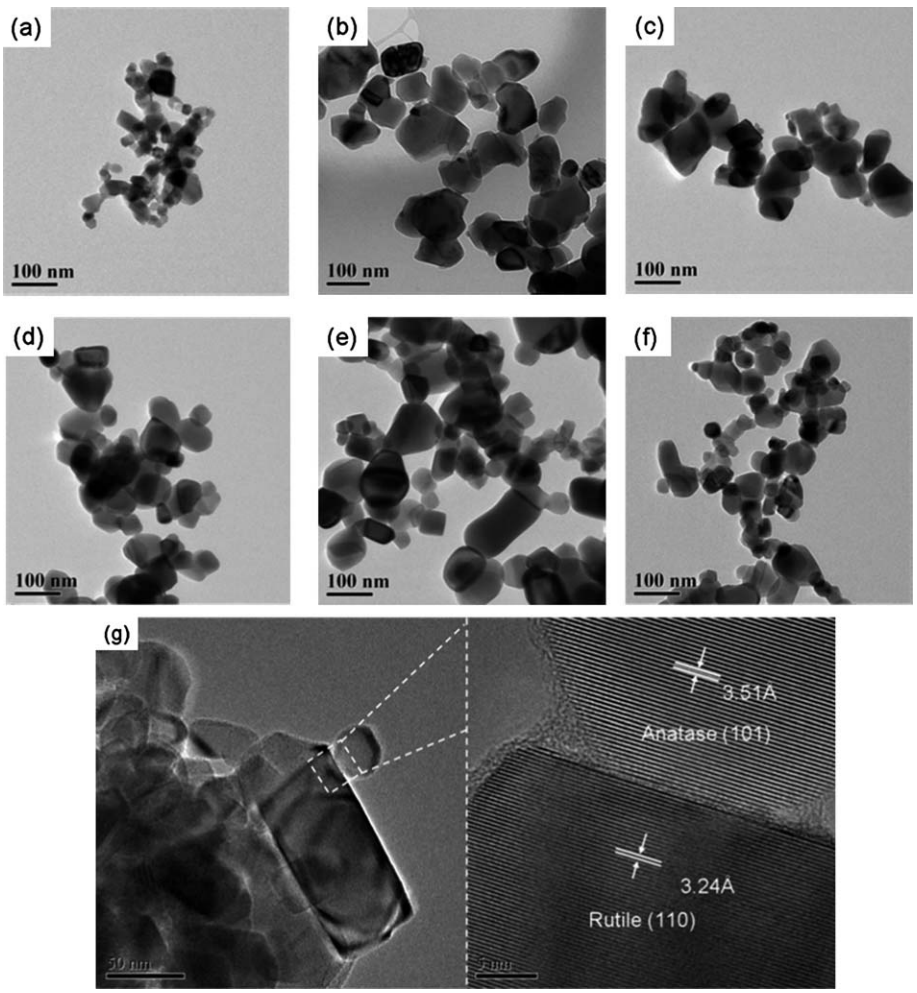

Fig. 4 TEM images of (a) P25, (b) P25-H_2O-700, (c) P25-0.1%SO_4^{2-}-700, (d) P25-0.5%SO_4^{2-}-700, (e) P25-1.0%SO_4^{2-}-700 and (f) P25-3.0%SO_4^{2-}-700. (g) HRTEM images of P25-1.0%SO_4^{2-}-700.

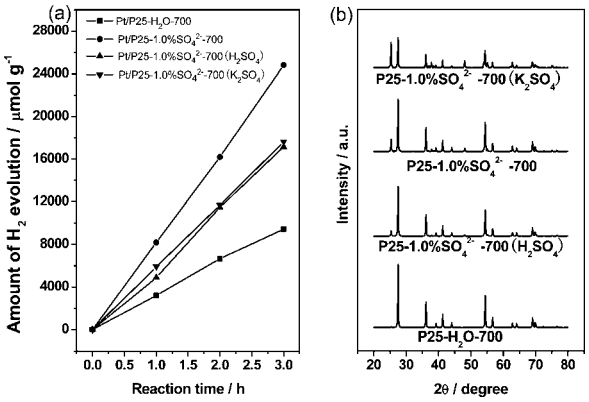

Fig. 5 (a) H_2 evolution activity and (b) XRD patterns of P25-H_2O-700, P25-1.0%SO_4^{2-}-700, P25-1.0%SO_4^{2-}-700(H_2SO_4) and P25-1.0%SO_4^{2-}-700(K_2SO_4).

the catalyst tuned by H_2SO_4 is insufficient while it is excessive by K_2SO_4.

In the experiments of this work, SO_4^{2-} has been used in the catalyst preparation to tune the surface phase structures of TiO_2. However, SO_4^{2-} might not be chemically bound to the surface of TiO_2 tightly, since some SO_4^{2-} are detected in the solution after the reaction. Previous investigations indicated that the presence of SO_4^{2-} in the reaction solution had little effect on the H_2 evolution activity of TiO_2.[40] Therefore, it is believed that the great enhancement of H_2 production shown in Fig. 2 is mainly ascribed to the change in the surface-phase structure of TiO_2 tuned by Na_2SO_4.

3.4. Suppressing CO formation and relation to the surface acidity of the catalysts

In order to meet the requirements for the direct application of H_2 in PEMFC, the CO concentration in H_2 should be rigorously controlled. In our experiments, CO selectivity (expressed as CO/H_2) for Pt/P25 is as high as 8500 ppm (Fig. 2(c)). However, it can be significantly decreased to around 30 ppm for Pt/P25-H_2O-700 and Pt/P25-x%SO_4^{2-}-700 catalysts.

It is proposed that CO is formed at the defect sites on the surface of TiO_2 *via* the dehydration reaction of the intermediate formic acid species.[40] Thermal treatment of P25 can efficiently reduce the defects in TiO_2 with enhancement of the crystallinity, which can lead to a significant suppression of CO formation. Fig. 3(b) shows that CO selectivity for Pt/P25-1.0%SO_4^{2-}-T is decreased with increasing the calcination temperature. Pt/P25-1.0%SO_4^{2-}-600 shows the highest CO selectivity while Pt/P25-1.0%SO_4^{2-}-800 exhibits the lowest, even lower than 10 ppm. These results indicate that the reducing CO selectivity may be due to the high crystallinity of the catalysts obtained by the high temperature calcination.

On the other hand, it is known that surface chemical properties are quite different between anatase and rutile. In particular, the surface Lewis acidity of the anatase phase is stronger than that of the rutile phase.[30,41] The difference in the phase composition of the samples could result in different surface acidity/basicity properties, which are usually critical issues for catalysis. In thermal catalysis, HCOOH decomposition on metal oxide may proceed in two pathways: dehydrogenation into H_2 and CO_2 occurring on basic oxides and dehydration into H_2O and CO occurring on acidic oxides. In other words, the reaction pathway is dependent on the acidity/basicity properties of the oxides in the thermal catalysis.[42–45] Therefore, the acidities of the samples in our experiments need to be investigated in detail.

FT-IR spectroscopy of pyridine adsorption was used to characterize the acidity of the samples. As presented in Fig. 6, five IR peaks are observed in the spectra. Two strong peaks at 1445 cm^{-1} and 1605 cm^{-1} correspond to the coordinated pyridine adsorbed on Lewis acid sites on TiO_2,[46–48] while the peaks at 1575 cm^{-1} and 1491 cm^{-1} are assigned to the vibrations of pyridine adsorbed on Brønsted acid sites and/or Lewis acid sites on TiO_2.[46–48] However, the characteristic peak of pyridine adsorbed on Brønsted acid sites on TiO_2 (at 1540 cm^{-1}) has not been observed. Therefore, the four peaks mentioned above should all correspond to the Lewis acid sites on TiO_2. In addition, another peak around 1593 cm^{-1} has been observed for P25-x%SO_4^{2-}-700 and the intensity increases with increasing the amount of SO_4^{2-}. It is speculated that this peak corresponds to the pyridine adsorption on the surface of TiO_2/SO_4^{2-}. Obviously, the most Lewis acid sites are detected for P25, while the intensities of IR peaks due to pyridine adsorbed on acid sites are sharply decreased for both P25-H_2O-700 and P25-x%SO_4^{2-}-700 samples with relatively less anatase phase.

Further, NH_3-TPD experiments have been carried out to investigate the acidity of the samples. It is noted that the NH_3-TPD profiles of the samples are quite different (Fig. 7). P25 shows one broad band centered at 400 °C ranging from 210 °C to 750 °C. The shape of the profile for P25-H_2O-700 is similar to that of P25 but with much weaker intensity, which indicates a smaller amount of acid sites existed. For P25-x%SO_4^{2-}-700, the addition of Na_2SO_4 makes the band of acid sites with medium acidity (centered at 400 °C) divide into two bands (centered at 350 °C and 450 °C). Moreover, a new band at 550 °C appears. Overall, the amount of medium acid sites, which are the indication of the number of intrinsic acid sites of TiO_2 itself, is dramatically reduced for both P25-H_2O-700 and P25-x%SO_4^{2-}-700 compared with that of P25. On the other hand, the amount of strong acid sites on P25-x%SO_4^{2-}-700 originating from the addition of SO_4^{2-} increases with increasing the amount of SO_4^{2-}.

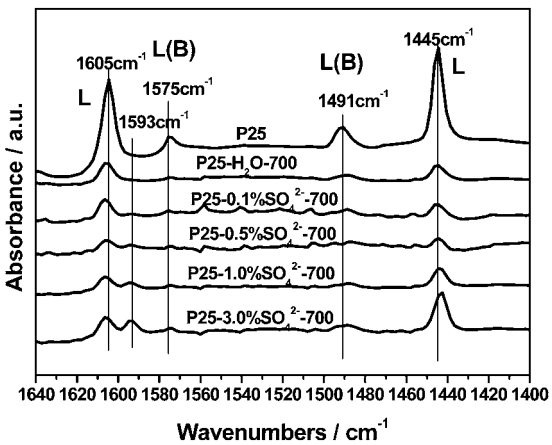

Fig. 6 IR spectra of pyridine adsorption on P25, P25-H_2O-700 and P25-x%SO_4^{2-}-700.

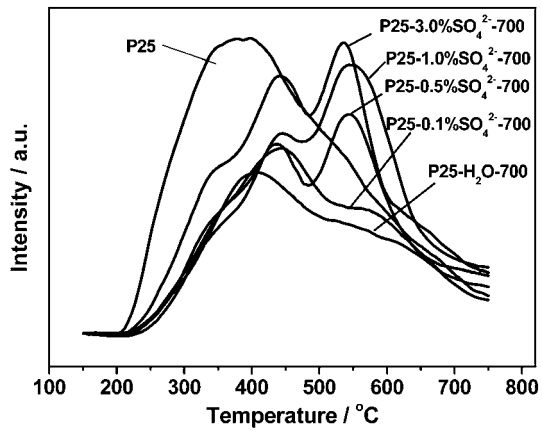

Fig. 7 NH_3-TPD profiles of P25, P25-H_2O-700 and P25-x%SO_4^{2-}-700.

P25 with the highest acidity corresponds to the highest CO selectivity, while other samples with decreased acidity correspond to lower CO selectivity. In summary, the pathway of HCOOH decomposition in the photocatalytic reactions investigated in this work is similar to that of thermal catalytic reaction. Namely, the surface acidity of the catalyst is responsible for the CO formation.

4. Conclusions

Commercial TiO_2 (P25), modified with SO_4^{2-} addition and calcined at high temperatures, exhibits an excellent H_2 production performance in photocatalytic reforming of methanol with Pt as a co-catalyst. The H_2 production activity of Pt/TiO_2-SO_4^{2-} can be increased up to 6 times the activity of Pt/P25. In addition, the CO concentration in the produced H_2 is decreased by two orders of magnitude compared with that of Pt/P25. The UV Raman spectra and the XRD patterns demonstrate that SO_4^{2-} can act as a stabilizer for the anatase phase resulting in a mixed phase structure of TiO_2, even after high temperature calcination. The surface-phase junctions formed between anatase and rutile, together with the high crystallinity of TiO_2, contribute to the excellent H_2 production activity. The IR spectra of pyridine adsorption and the NH_3-TPD profiles of the catalysts indicate that the decrease in the surface acidity of TiO_2 could be responsible for the low CO selectivity.

Acknowledgements

We acknowledge the financial support for this work from the National Natural Science Foundation of China (NSFC, grant no. 21090340/21090341, 21061140361), the National Basic Research Program of China (grant no. 2009CB220010) and the Solar Energy Action Plan of Chinese Academy of Sciences (grant no. KGCX2-YW-391-1).

Notes and references

1 A. Kudo and Y. Miseki, *Chem. Soc. Rev.*, 2009, **38**, 253.
2 R. D. Cortright, R. R. Davda and J. A. Dumesic, *Nature*, 2002, **418**, 964.
3 R. C. Saxena, D. K. Adhikari and H. B. Goyal, *Renewable Sustainable Energy Rev.*, 2009, **13**, 156.
4 H. Balat and E. Kirtay, *Int. J. Hydrogen Energy*, 2010, **35**, 7416.
5 S. Sa, H. Silva, L. Brandao, J. M. Sousa and A. Mendes, *Appl. Catal., B*, 2010, **99**, 43.
6 Y. Matsumura and H. Ishibe, *J. Catal.*, 2009, **268**, 282.
7 D. R. Palo, R. A. Dagle and J. D. Holladay, *Chem. Rev.*, 2007, **107**, 3992.
8 P. P. C. Udani, P. V. D. S. Gunawardana, H. C. Lee and D. H. Kim, *Int. J. Hydrogen Energy*, 2009, **34**, 7648.
9 M. Bowker, L. Millard, J. Greaves, D. James and J. Soares, *Gold Bull.*, 2004, **37**, 170.
10 G. L. Chiarello, M. H. Aguirre and E. Selli, *J. Catal.*, 2010, **273**, 182.
11 Z. G. Li, Y. X. Wang, J. W. Liu, G. Chen, Y. X. Li and C. Zhou, *Int. J. Hydrogen Energy*, 2009, **34**, 147.
12 T. Miwa, S. Kaneco, H. Katsumata, T. Suzuki, K. Ohta, S. C. Verma and K. Sugihara, *Int. J. Hydrogen Energy*, 2010, **35**, 6554.
13 L. S. Al-Mazroai, M. Bowker, P. Davies, A. Dickinson, J. Greaves, D. James and L. Millard, *Catal. Today*, 2007, **122**, 46.
14 H. Tada and M. Tanaka, *Langmuir*, 1997, **13**, 360.
15 Z. Ding, G. Q. Lu and P. F. Greenfield, *J. Phys. Chem. B*, 2000, **104**, 4815.
16 G. H. Li and K. A. Gray, *Chem. Phys.*, 2007, **339**, 173.
17 J. Zhang, Q. Xu, Z. C. Feng, M. J. Li and C. Li, *Angew. Chem., Int. Ed.*, 2008, **47**, 1766.
18 Q. Xu, Y. Ma, J. Zhang, X. L. Wang, Z. C. Feng and C. Li, *J. Catal.*, 2011, **278**, 329.
19 C. M. Ronconi, C. Ribeiro, L. O. S. Bulhoes and E. C. Pereira, *J. Alloys Compd.*, 2008, **466**, 435.
20 L. Y. Wang, Y. P. Sun and B. S. Xu, *J. Mater. Sci.*, 2008, **43**, 1979.
21 D. S. Hwang, N. H. Lee, D. Y. Lee, J. S. Song, S. H. Shin and S. J. Kim, *Smart Mater. Struct.*, 2006, **15**, 74.
22 A. Testino, I. R. Bellobono, V. Buscaglia, C. Canevali, M. D'Arienzo, S. Polizzi, R. Scotti and F. Morazzoni, *J. Am. Chem. Soc.*, 2007, **129**, 3564.
23 H. P. Xu, Y. P. Sun, J. W. Wang, H. Q. Zhan and X. M. Chen, *Rare Metal Mater. Eng.*, 2005, **34**, 1089.
24 M. C. Yan, F. Chen, J. L. Zhang and M. Anpo, *J. Phys. Chem. B*, 2005, **109**, 8673.
25 G. Colon, M. C. Hidalgo and J. A. Navio, *Appl. Catal., B*, 2003, **45**, 39.
26 J. Z. Zhang, Z. M. Liu and J. G. Goodwin, *J. Power Sources*, 2010, **195**, 3060.
27 R. J. Bellows, E. P. MarucchiSoos and D. T. Buckley, *Ind. Eng. Chem. Res.*, 1996, **35**, 1235.
28 A. A. Gribb and J. F. Banfield, *Am. Mineral.*, 1997, **82**, 717.
29 J. Zhang, M. J. Li, Z. C. Feng, J. Chen and C. Li, *J. Phys. Chem. B*, 2006, **110**, 927.
30 W. G. Su, J. Zhang, Z. C. Feng, T. Chen, P. L. Ying and C. Li, *J. Phys. Chem. C*, 2008, **112**, 7710.
31 J. Y. Shi, J. Chen, Z. C. Feng, T. Chen, Y. X. Lian, X. L. Wang and C. Li, *J. Phys. Chem. C*, 2007, **111**, 693.
32 D. C. Hague and M. J. Mayo, *Nanostruct. Mater.*, 1993, **3**, 61.
33 K. N. P. Kumar, K. Keizer, A. J. Burggraaf, T. Okubo, H. Nagamoto and S. Morooka, *Nature*, 1992, **358**, 48.
34 A. Orendorz, A. Brodyanski, J. Losch, L. H. Bai, Z. H. Chen, Y. K. Le, C. Ziegler and H. Gnaser, *Surf. Sci.*, 2007, **601**, 4390.
35 T. L. Thompson and J. T. Yates, *Chem. Rev.*, 2006, **106**, 4428.
36 H. Nakajima, T. Mori, Q. Shen and T. Toyoda, *Chem. Phys. Lett.*, 2005, **409**, 81.
37 T. Kawahara, Y. Konishi, H. Tada, N. Tohge, J. Nishii and S. Ito, *Angew. Chem., Int. Ed.*, 2002, **41**, 2811.
38 S. Leytner and J. T. Hupp, *Chem. Phys. Lett.*, 2000, **330**, 231.
39 D. C. Hurum, A. G. Agrios, K. A. Gray, T. Rajh and M. C. Thurnauer, *J. Phys. Chem. B*, 2003, **107**, 4545.
40 G. P. Wu, T. Chen, X. Zong, H. J. Yan, G. J. Ma, X. L. Wang, Q. Xu, D. E. Wang, Z. B. Lei and C. Li, *J. Catal.*, 2008, **253**, 225.
41 M. Primet, P. Pichat and M. V. Mathieu, *J. Phys. Chem.*, 1971, **75**, 1221.
42 P. Mars, J. J. F. Scholten and P. Zwietering, *Adv. Catal.*, 1963, **14**, 35.
43 G. Munuera, *J. Catal.*, 1970, **18**, 19.
44 S. A. Halawy, S. S. Al-Shihry and M. A. Mohamed, *Catal. Lett.*, 1997, **48**, 247.
45 Y. Uemura, T. Taniike, M. Tada, Y. Morikawa and Y. Iwasawa, *J. Phys. Chem. C*, 2007, **111**, 16379.
46 O. M. Busch, W. Brijoux, S. Thomson and F. Schuth, *J. Catal.*, 2004, **222**, 174.
47 M. Kobayashi, A. Morita and M. Ikeda, *Appl. Catal., B*, 2007, **71**, 94.
48 X. C. Wang, J. C. Yu, P. Liu, X. X. Wang, W. Y. Su and X. Z. Fu, *J. Photochem. Photobiol., A*, 2006, **179**, 339.